Raman tensor elements of wurtzite ZnO

T. Sander,* S. Eisermann, B. K. Meyer, and P. J. Klar
Institute of Experimental Physics I, Justus-Liebig-University, Giessen, Germany
(Received 9 February 2012; revised manuscript received 16 March 2012; published 23 April 2012)

The angle dependence of the phonon modes of *a*-plane ($11\bar{2}0$) and *c*-plane (0001) faced ZnO crystals in wurtzite structure was studied at room temperature by Raman spectroscopy in backscattering geometry. The samples were rotated by 360° about the axis defined by the excitation laser light coming in at normal incidence. A polarization filter combined with a $\lambda/2$ plate was used in the optical path of the scattered light from the sample to select parallelly or perpendicularly polarized light with respect to the linearly polarized 532 nm excitation laser. The origin of the observed Raman modes is discussed in detail, and their variations in intensity are compared to calculated scattering intensities of allowed phonon modes in wurtzite crystals, yielding the Raman tensor elements of several modes normalized to that of the E_2^{high} phonon mode: $|a/d| = 0.6$ and $|b/d| = 0.5$, $|c/d| = 0.4$, and $|a/d| = 0.1$ for the A_1(TO), E_1(TO), and A_1(LO) phonon modes, respectively.

DOI: 10.1103/PhysRevB.85.165208 PACS number(s): 63.20.−e, 78.30.Fs

I. INTRODUCTION

Raman spectroscopy yields information about the symmetry and frequencies of vibrational modes in crystals. Variations in phonon mode intensities and frequencies can be used to study the crystal quality and structure as well as to prove the existence of defects and impurities. Angle-dependent Raman spectra reveal the symmetry of the vibrational modes and thus the symmetry of the material under study.

The first Raman spectra of wurtzite ZnO were published by Damen *et al*. and Arguello *et al*., who determined the fundamental vibrational modes of ZnO crystals in the 1960s.[1,2] Since then, Raman spectra of ZnO have been studied intensively.[3–5] Resonant Raman spectroscopy was performed by Scott[6] and Calleja and Cardona.[7] The influence of temperature effects on the Raman modes in ZnO can be found in Refs. 8 and 9, and pressure dependence was studied by Mitra *et al*., Decremps *et al*., and recently by Reparaz *et al*., who clarified the effect of hydrostatic pressure on the LO-TO splitting of the polar modes A_1 and E_1.[10–12] Callsen *et al*. investigated uniaxial pressure.[13] An *ab initio* calculation of the influence of pressure on the Raman modes was carried out by Serrano *et al*.[14] Furthermore there is an increasing number of publications concerning the influence of confinement on the vibrational properties of ZnO, for example, Refs. 15–18. Surprisingly, some questions still remain, such as the determination of ZnO Raman tensor elements and the unambiguous identification of some of the phonon modes.

In this article, we calculated the angle variations of the Raman intensities of allowed phonon modes in crystals with wurtzite structure by parameterizing the incoming and scattered polarization vectors and compared those results with experimental data extracted from angle-dependent Raman spectra of ZnO crystals of different orientations. This allows us to give a full mode assignment and to determine the Raman tensor elements of wurtzite ZnO.

II. EXPERIMENTAL DETAILS

Two ZnO samples were investigated: one commercially acquired *a*-plane substrate from Crystec and one *c*-plane sample, which was grown by chemical vapor deposition (CVD) in a vertical reactor at 375 °C on a *c*-plane, single-crystal ZnO substrate. As a metallic precursor, zinc shots were evaporated and transported to the reaction zone by inert gas. As an oxygen precursor, gaseous NO_2 was utilized. The working pressure was 4 mbar.

The Raman spectra were recorded in backscattering geometry at room temperature. A polarized 532 nm excitation laser was focused with a 50× objective onto the sample surface. The same objective was used to collect the scattered light, which was then dispersed by a spectrometer with a focal length of 250 mm and detected by a CCD. The system's spectral resolution is limited to 1.5 cm^{-1}. In the optical path of the scattered light, a polarizer was inserted, enabling the measurement of the component of the scattered light with polarization parallel to that of the incoming laser light. Combining the polarizer with a $\lambda/2$ plate allows the detection of the perpendicularly polarized component of the scattered light. To measure the angle-dependent spectra, a microscope stage rotated about the axis defined by the direction of the incoming excitation laser was used.

III. RAMAN SELECTION RULES FOR WURTZITE CRYSTALS

The wurtzite crystal structure possesses four atoms per primitive unit cell, leading to nine optical and three acoustic phonon branches. It belongs to the C_{6v} point group (see Ref. 1, for example). In the point group notation, the nine zone-center optical phonon mode symmetries are

$$A_1 \oplus 2B_1 \oplus E_1 \oplus 2E_2. \quad (1)$$

According to group theory, the A_1 phonon branch is polarized along the z direction (see Fig. 1 for a reference coordinate system) and is both Raman- and infrared-active. The E_1 branch is also Raman- and infrared-active but twofold degenerate, and its phonons are polarized in the xy plane. Also twofold degenerate is the E_2 phonon, which is Raman-active only while the two B_1 modes are silent modes. Of course the symmetry considerations strictly only hold at $k = 0$. Raman modes with A_1 and E_1 symmetry exhibit shifts of the mode frequency due to bond polarity, i.e., depending on the mode being longitudinal (LO) or transversal (TO).

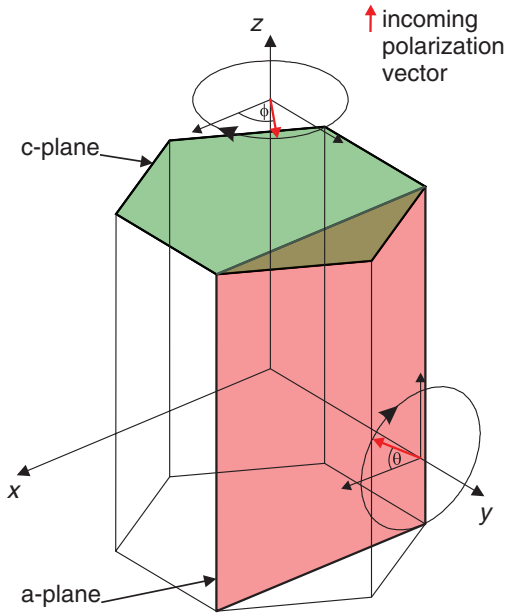

FIG. 1. (Color online) Schematic illustration of the hexagonal wurtzite crystal structure and the coordinate system used. The red rectangle represents one of the a-planes which are perpendicular to the a axes, and the green hexagon represents the c-plane which is perpendicular to the optical axis. The red arrows denote the polarization vectors of the incoming light, and the circles around the polarization vectors describe their rotation, where θ and ϕ are the rotation angles with respect to the x axis.

The scattering intensities in a Raman experiment are given by

$$I_s \propto |\vec{e}_i \cdot \boldsymbol{R} \cdot \vec{e}_s|^2, \tag{2}$$

where $\vec{e}_i$ and $\vec{e}_s$ are the polarization vectors of the incident and scattered radiation, respectively, and $\boldsymbol{R}$ is the complex second-rank Raman tensor.[19] Group theory yields elements of the latter which are zero; the remaining ones may be nonzero and can be determined by experiment. For the C_{6v} point group corresponding to the wurtzite structure one obtains[19]

$$\boldsymbol{R}[A_1(z)] = \begin{pmatrix} a & 0 & 0 \\ 0 & a & 0 \\ 0 & 0 & b \end{pmatrix}, \tag{3}$$

$$\boldsymbol{R}[E_1(-x)] = \begin{pmatrix} 0 & 0 & -c \\ 0 & 0 & 0 \\ -c & 0 & 0 \end{pmatrix}, \tag{4}$$

$$\boldsymbol{R}[E_1(y)] = \begin{pmatrix} 0 & 0 & 0 \\ 0 & 0 & c \\ 0 & c & 0 \end{pmatrix}, \tag{5}$$

$$\boldsymbol{R}[E_2] = \begin{pmatrix} d & d & 0 \\ d & -d & 0 \\ 0 & 0 & 0 \end{pmatrix} = \begin{pmatrix} 0 & d & 0 \\ d & 0 & 0 \\ 0 & 0 & 0 \end{pmatrix} + \begin{pmatrix} d & 0 & 0 \\ 0 & -d & 0 \\ 0 & 0 & 0 \end{pmatrix}. \tag{6}$$

The Raman tensor of the E_2 phonon branch is degenerate and can be divided into two matrices, as shown above. Each of the matrices represents an E_2 eigenmode.

If the orientation of the crystal axes is known, one may align the sample and the polarized excitation laser in such a manner that the incoming polarization vector is a simple unit vector. For example, if polarized light from the excitation laser propagates parallel to the c axis, and thus onto the c-plane surface, the polarization vector in reference to the crystal coordinate system lies in the xy plane. Using polar coordinates, the incident polarization vector has the form

$$\vec{e}_{i,c} = \begin{pmatrix} \cos(\phi) \\ \sin(\phi) \\ 0 \end{pmatrix}, \tag{7}$$

where ϕ is the angle between $\vec{e}_{i,c}$ and the x axis; see Fig. 1. In conclusion, the polarization vectors for the scattered light are in backscattering geometry,

$$\vec{e}^{\,\parallel}_{s,c} = \begin{pmatrix} \cos(\phi) \\ \sin(\phi) \\ 0 \end{pmatrix} \tag{8}$$

and

$$\vec{e}^{\,\perp}_{s,c} = \begin{pmatrix} -\sin(\phi) \\ \cos(\phi) \\ 0 \end{pmatrix}, \tag{9}$$

where $\parallel$ and $\perp$ denote parallel and perpendicular polarization in reference to the polarization of the incident laser light, respectively. In the Porto notation, rotations of the c-plane sample in the two polarization configurations can be represented by $z(xx)\bar{z} \leftrightarrow z(yy)\bar{z}$ and $z(xy)\bar{z} \leftrightarrow z(yx)\bar{z}$, respectively, where the symbols outside the parentheses denote the propagation directions of the incoming and scattered light.[1] The polarization of the incident and scattered radiation is given by the two symbols inside the parentheses.

In case of an a-plane sample, the polarization of the excitation laser can be chosen to lie in the xz plane:

$$\vec{e}_{i,a} = \begin{pmatrix} \cos(\theta) \\ 0 \\ \sin(\theta) \end{pmatrix}. \tag{10}$$

Here θ is the angle between $\vec{e}_{i,a}$ and the x axis. The scattered vectors can be derived in analogy to the c-plane case. Following the Porto notation, the parallel and perpendicular configurations of the polarization vectors for an a-plane sample are written as $y(xx)\bar{y} \leftrightarrow y(zz)\bar{y}$ and $y(xz)\bar{y} \leftrightarrow y(zx)\bar{y}$. In Fig. 1, the rotating polarization vectors are sketched with respect to the hexagonal crystal structure.

Inserting the Raman tensors (3) to (6) and the polarization vectors into Eq. (2) yields the angle-dependent selection rules for symmetry-allowed Raman modes. The E_2 phonon branch requires special consideration. Since its Raman tensor corresponds to two independent modes, the scattering intensity for each matrix has to be calculated independently using Eq. (2). The total scattering efficiency for the E_2 phonon is then the sum of these two results.[19] The selection rules for different sample orientations and scattering geometries are summarized in Table I. In cases (such as for the E_1 and E_2 modes) where all the nonzero tensor elements are equal, the Raman tensor may be chosen to be real. If the Raman tensor contains nonzero

TABLE I. Selection rules for the allowed Raman modes of a- and c-plane faced crystals of wurtzite structure for different polarizations of the incident $\vec{e}_i$ and scattered $\vec{e}_s$ polarization vectors: parallel ($\vec{e}_i \parallel \vec{e}_s$) and perpendicular ($\vec{e}_i \perp \vec{e}_s$), where θ is the angle between $\vec{e}_i$ and the x axis (see Fig. 1) and χ is the phase difference between the complex Raman tensor elements a and b.

	a-plane		c-plane	
Raman mode	$\vec{e}_i \parallel \vec{e}_s$ $y(xx)\bar{y} \leftrightarrow y(zz)\bar{y}$	$\vec{e}_i \perp \vec{e}_s$ $y(xz)\bar{y} \leftrightarrow y(zx)\bar{y}$	$\vec{e}_i \parallel \vec{e}_s$ $z(xx)\bar{z} \leftrightarrow z(yy)\bar{z}$	$\vec{e}_i \perp \vec{e}_s$ $z(xy)\bar{z} \leftrightarrow z(yx)\bar{z}$
$A_1(z)$	$\lvert a\rvert^2 \cos^4(\theta) + \lvert b\rvert^2 \sin^4(\theta)$ $+1/2\lvert a\rvert\lvert b\rvert \cos(\chi)\sin^2(2\theta)$	$1/4 \sin^2(2\theta)[\lvert a\rvert^2$ $+\lvert b\rvert^2 - 2\lvert a\rvert\lvert b\rvert \cos(\chi)]$	$\lvert a\rvert^2$	0
$E_1(-x)$	$\lvert c\rvert^2 \sin^2(2\theta)$	$\lvert c\rvert^2 \cos^2(2\theta)$	0	0
$E_1(y)$	0	0	0	0
E_2	$\lvert d\rvert^2 \cos^4(\theta)$	$\lvert d\rvert^2 \sin^2(\theta)\cos^2(\theta)$	$\lvert d\rvert^2$	$\lvert d\rvert^2$

tensor elements which are not related by symmetry, these may differ by a complex phase factor. Here, this is the case for the A_1 phonon mode, which is also sensitive to the phase difference χ between the complex tensor elements a and b, thus making χ accessible by experiment. If the coordinate system is chosen such that the x axis is perpendicular to an a-plane instead of the y axis, the same angle variations hold as shown in Table I; only the behavior of the $E_1(-x)$ phonon is interchanged with that of the $E_1(y)$ mode. Based on these results and the possible phonon propagation directions, the allowed Raman modes for different configurations are given in Table II in a more convenient way.

IV. RESULTS AND DISCUSSION

A. Angle-dependent Raman spectra of ZnO

In Fig. 2(a), the Raman spectra of the a-plane ZnO sample in the range of 150 to 750 cm^{-1} are shown for different rotation angles and for parallel polarization vectors of the excitation laser and the scattered light [$y(xx)\bar{y} \leftrightarrow y(zz)\bar{y}$]. For clarity, the spectra are shifted on the y axis by a constant amount. The three modes located at around 379, 412, and 439 cm^{-1} are the allowed Raman-active phonon modes A_1(TO), E_1(TO), and E_2^{high}, respectively. Between 0° and 180° the E_2^{high} mode reaches a single intensity maximum at about 90° [see Fig. 4(c)], whereas the E_1(TO) mode has two maxima, 40° and 120°, and three minima, 0°, 90° [not shown in Fig. 2(a) but shown in Fig. 4(c)], and 180°. Compared to the E_1(TO) phonon, the A_1(TO) mode is phase shifted by 90°, being maximal when E_1(TO) is minimal and vice versa, but it never disappears completely. The origin of the fourth dominant, broad feature in the spectra located at 332 cm^{-1}, which follows the angular variations of the A_1(TO) phonon, is controversially discussed in the literature. Calleja and Cardona attributed it to a two-phonon process from the K-M-Σ branch of the dispersion relation around 160 cm^{-1}, whereas Cuscó *et al.* suggested, based on temperature-dependent Raman measurements, that it is a difference mode between E_2^{high} and E_2^{low}.[7,9] The E_2^{low} phonon, located at around 101 cm^{-1}, is not observable in the Raman shift range considered here, and the A_1(LO) (575 cm^{-1}) is not allowed; see Table II.

TABLE II. Allowed Raman modes in crystals with wurtzite structure for different polarization and propagation directions considered in this work. Here ***θ*** stands for angle-dependent modes, a dash (–) stands for symmetry-forbidden modes, and ***c*** stands for constant Raman modes.

		Scattering geometry			
Raman mode		$y(xx)\bar{y} \leftrightarrow y(zz)\bar{y}$	$y(xz)\bar{y} \leftrightarrow y(zx)\bar{y}$	$z(xx)\bar{z} \leftrightarrow z(yy)\bar{z}$	$z(xy)\bar{z} \leftrightarrow z(yx)\bar{z}$
$A_1(z)$	LO	–	–	***c***	–
	TO	***θ***	***θ***	–	–
$E_1(-x)$	LO	–	–	–	–
	TO	***θ***	***θ***	–	–
$E_1(y)$	LO	–	–	–	–
	TO	–	–	–	–
E_2		***θ***	***θ***	***c***	***c***

The Raman spectra for crossed polarization vectors [$y(xz)\bar{y} \leftrightarrow y(zx)\bar{y}$] for different rotation angles are shown in Fig. 2(b). In the insets of Figs. 2(a) and 2(b), enlargements of two Raman shift ranges are shown, in which the spectra are shifted by a smaller constant amount compared to the original ones for clarity. Due to its frequency the feature at around 590 cm^{-1} may be attributed to the E_1(LO) phonon mode, although it was shown in the last section (see Table II) that this phonon mode is forbidden in the scattering geometry studied here. The reason for its occurrence as a weak signal may be deviations from an ideal geometry, such as a tilted sample or outer rays from the microscope objective leading to a constant component p of the polarization vector along the normal axis of the sample's surface; see Fig. 3. Using the latter ansatz, the polarization vectors for the incident and scattered light of an a-plane sample have the new form

$$\vec{e}_{i,a} = \frac{1}{\sqrt{1+p^2}} \begin{pmatrix} \cos(\theta) \\ p \\ \sin(\theta) \end{pmatrix}, \tag{11}$$

$$\vec{e}_{s,a}^{\,\parallel} = \vec{e}_{i,a}, \tag{12}$$

and

$$\vec{e}_{s,a}^{\,\perp} = \frac{1}{\sqrt{1+p^2}} \begin{pmatrix} -\sin(\theta) \\ p \\ \cos(\theta) \end{pmatrix}. \tag{13}$$

(Note that the vectors $\vec{e}_{i,a}$ and $\vec{e}_{s,a}^{\,\perp}$ are not perpendicular to each other any longer due to the deviations from a perfect

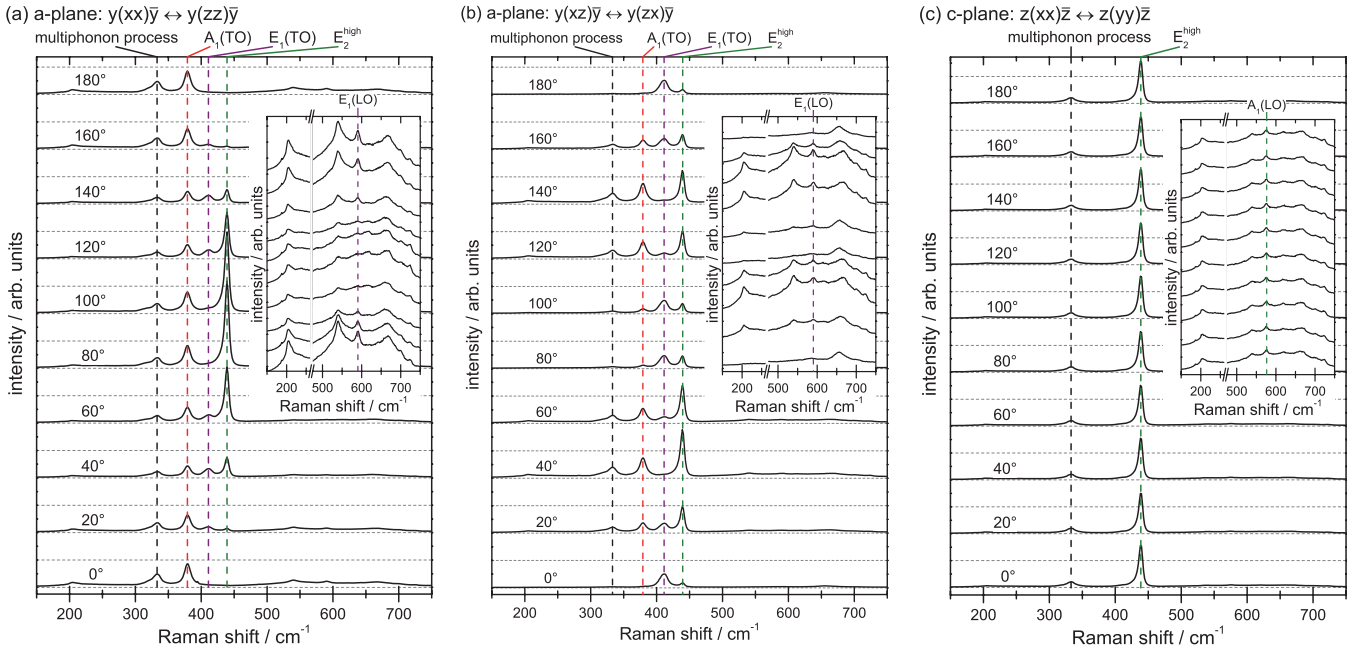

FIG. 2. (Color online) (a) and (b) show the Raman spectra of the a-plane faced sample for different rotation angles, shifted by a constant amount, for parallel $[y(xx)\bar{y} \leftrightarrow y(zz)\bar{y}]$ and perpendicular $[y(xz)\bar{y} \leftrightarrow y(zx)\bar{y}]$ alignment of the polarization vectors. The spectra of the c-plane sample in (c) were recorded for parallel alignment of the polarization vectors $[z(xx)\bar{z} \leftrightarrow z(yy)\bar{z}]$. Enlargements of two Raman shift ranges are plotted in each graph for rotation angles from 0° to 180° in 20° steps. For clarity, the spectra in the insets are shifted by a smaller amount. Dominant modes in the spectra are labeled.

geometry.) Inserting these polarization vectors and the Raman tensors for wurtzite crystals (3) to (6) into Eq. (2) yields to nonzero intensity of the $E_1(y)$ phonon mode representing the E_1(LO) mode in the coordinate system chosen in this work (see Fig. 1):

$$I^{\parallel}[E_1(y)] \propto \left| \frac{2cp\sin(\theta)}{1+p^2} \right|^2, \tag{14}$$

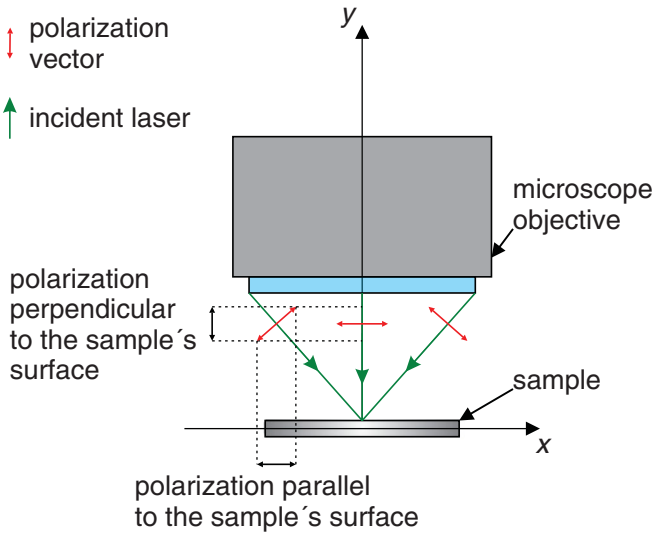

FIG. 3. (Color online) Schematic drawing of outer rays from a microscope objective leading to a component of the polarization vector along an axis perpendicular to the sample's surface.

$$I^{\perp}[E_1(y)] \propto \left| \frac{cp(\sin(\theta)+\cos(\theta))}{1+p^2} \right|^2. \tag{15}$$

As long as p is small, its influence on the angle dependence of the intensities of the other three Raman modes in wurtzite crystals is negligible.

The intensity of the E_1(LO) signal is plotted in Figs. 4(a) and 4(b) versus the rotation angle, being well described by Eqs. (14) and (15) (dash-dotted lines in the figures) after subtracting a $[\sin^2(2\theta) + y]$ angle-dependent background. To demonstrate the angle variations of the background, signals close in Raman shift to the E_1(LO) phonon at 574 and 570 cm^{-1} are included in Figs. 4(a) and 4(b). All other features in the insets in Figs. 2(a) and 2(b), for example, at about 205 or 540 cm^{-1}, correspond to multiphonon processes showing a somewhat similar angular variation as the background. Assignments of those signals can be found in Refs. 1–3 and 9 but are contested due to the relaxed selection rules in two or more phonon processes.

In Fig. 2(c) the spectra for parallel polarization vectors from the c-plane ZnO sample $[z(xx)\bar{z} \leftrightarrow z(yy)\bar{z}]$ are plotted. These reveal three dominant, angle-independent peaks: the above-discussed multiphonon process at 332 cm^{-1}, the A_1(LO) mode (575 cm^{-1}), and the E_2^{high} phonon mode (439 cm^{-1}). The constant angle dependence of the two allowed phonon modes is in agreement with the calculated selection rules summarized in Table I. According to Callender *et al.* the low intensity of the A_1(LO) signal, observable in the inset of Fig. 2(c), is due to a suppression caused by destructive interference of the deformation potential with the Fröhlich contributions.[3]

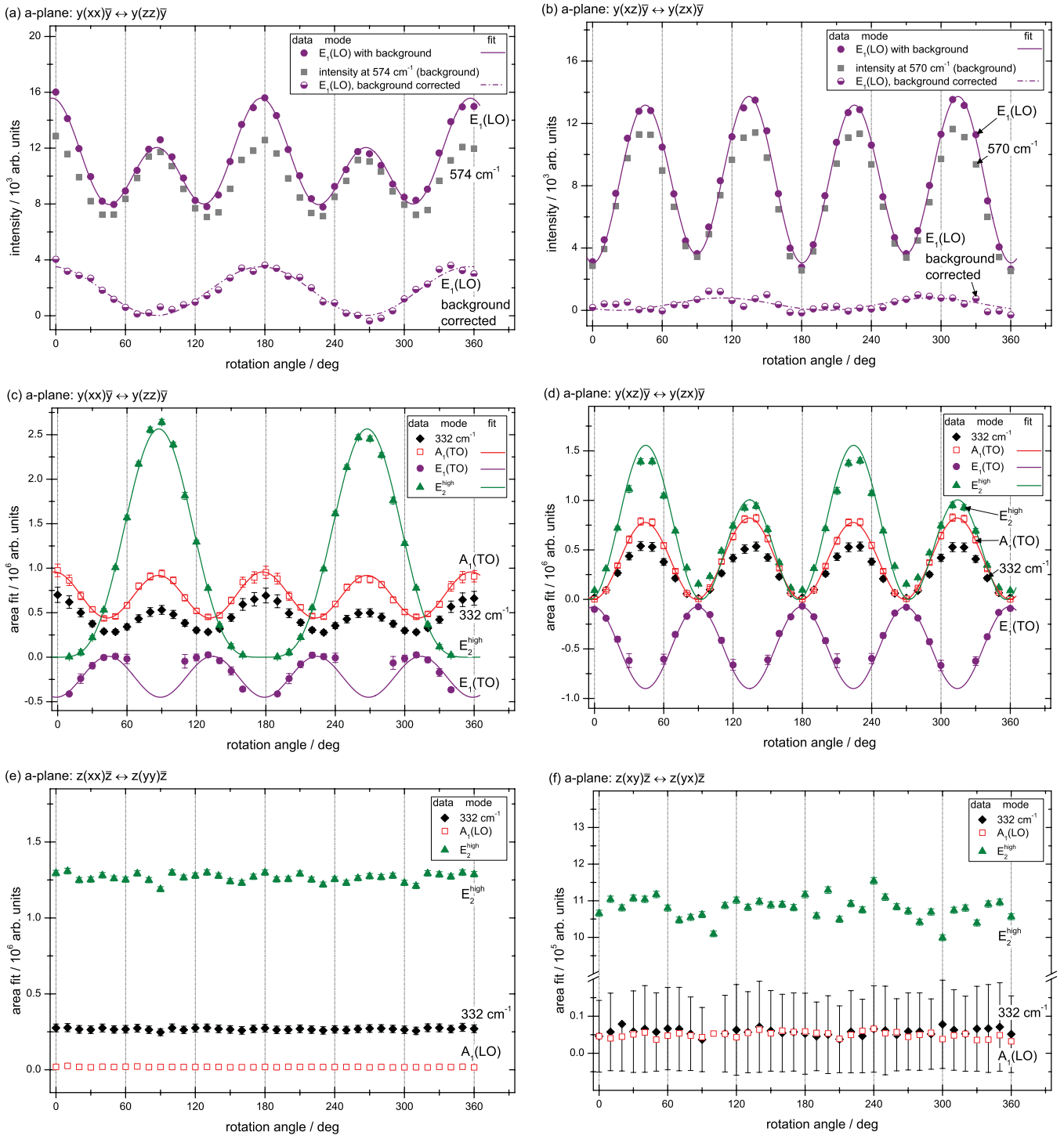

FIG. 4. (Color online) (a) and (b) show the intensity of the forbidden E_1(LO) signal from the a-plane ZnO sample vs the rotation angle for parallel and perpendicular polarization vectors, respectively. Signals close in Raman shift to the E_1(LO) mode are included, giving the angular dependence of the background. The dash-dotted lines are fits to the observed angle dependences based on Eqs. (14) and (15), describing deviations from a perfect geometry due to outer rays from the microscope objective. In (c) and (d) the integrated area of the dominant features in the Raman spectra from the a-plane sample vs the rotation angle for parallel and crossed polarization vectors are plotted. For a better overview the E_1(TO) signal is shifted down in both cases by a constant amount. The integrated areas of the dominant features from the c-plane sample for both polarization configurations are given in (e) and (f). The error bars are the standard errors of the integrated area, the solid lines in (c) are fits to the observed angle dependences based on the functions in Table I, and the fits in (d) were calculated using the polarization vectors in (16) and (17), which depend on the angle between the polarization filter and the $\lambda/2$ plate.

TABLE III. Ratio of the Raman tensor elements of several phonon modes of ZnO estimated from the parameters of fits to angle-dependent Raman spectra for two different alignments of the incident $\vec{e}_i$ and scattered $\vec{e}_s$ polarization vectors. All tensor elements are normalized to that of the E_2^{high} mode.

	Tensor element		$\vec{e}_i \parallel \vec{e}_s$	$\vec{e}_i \perp \vec{e}_s$
a-plane	A_1(TO)	$\lvert a/d\rvert$	0.611 ± 0.006	0.585 ± 0.022
	A_1(TO)	$\lvert b/d\rvert$	0.599 ± 0.005	0.413 ± 0.039
	E_1(TO)	$\lvert c/d\rvert$	0.424 ± 0.004	0.404 ± 0.001
	E_2^{high}	$\lvert d/d\rvert$	1.000 ± 0.002	1.000 ± 0.004
c-plane	A_1(LO)	$\lvert a/d\rvert$	0.121 ± 0.001	
	E_2^{high}	$\lvert d/d\rvert$	1.000 ± 0.002	

The inset further reveals several constant structures due to multiphonon processes.

B. ZnO Raman tensor elements

The dominant features in the measured spectra were fitted with combinations of Gaussian and Lorentzian functions assuming a linear background in the range of 275 to 525 cm^{-1} and in a narrow range around the A_1(LO) phonon signal, chosen individually for each spectrum. In fact the E_2^{high} mode is best described with a Fano-like lineshape due to its decay into a sum of longitudinal and transverse acoustic phonons.[9,20] However, fitting with a Fano-like lineshape does not improve our results of the peak positions and integrated areas since our spectral resolution is limited to 1.5 cm^{-1} and the assumption of a linear background for the fitting process is the dominant source of error. The results of these fits are shown in Figs. 4(c)–4(f), in which the integrated area of each signal is plotted versus the rotation angle for the two polarization geometries. The error bars are the standard errors of the integrated area. Due to the fitting routine, the standard error of the Gaussian functions could not be estimated. In these cases the largest observed standard error of that mode of fits with Lorentzian functions was used as an upper limit. To determine the Raman tensor elements, the angle variations were fitted with the functions calculated in Sec. III weighted by the standard errors of the integrated area.

In the case of perpendicular polarization vectors of the excitation laser and the scattered light from the samples, the results of Sec. III needed to be corrected due to an imperfect alignment of the polarization filter and the $\lambda/2$ plate, leading to the detection of parallelly and perpendicularly polarized light simultaneously. This is clearly observable in Fig. 4(d) for the E_2^{high} phonon mode, which is expected to have a 90° symmetry but reveals a 180° one. Furthermore the A_1(LO) mode, forbidden in $z(xy)\bar{z} \leftrightarrow z(yx)\bar{z}$ geometry, is visible in the data shown in Fig. 4(f). To account for this deviation, the scattered polarization vectors have to be modified to

$$\vec{e}_{s,a}^{\perp} = \begin{pmatrix} \cos(\theta)\sin\alpha - \sin(\theta)\cos\alpha \\ 0 \\ \sin(\theta)\sin\alpha + \cos(\theta)\cos\alpha \end{pmatrix} \tag{16}$$

and

$$\vec{e}_{s,c}^{\perp} = \begin{pmatrix} \cos(\phi)\sin\alpha - \sin(\phi)\cos\alpha \\ \sin(\phi)\sin\alpha + \cos(\phi)\cos\alpha \\ 0 \end{pmatrix}, \tag{17}$$

where α is the tilt angle between the polarization filter and the $\lambda/2$ plate. The solid lines in Fig. 4(c) are based upon the functions in Table I, whereas the lines in Fig. 4(d) were calculated with the corrected polarization vectors (16) and (17).

The misalignment of the polarization filter and the $\lambda/2$ plate was estimated with the help of the fits to less than 7°. The ratios of the fit parameters yield the relative values of the Raman tensor elements for ZnO, summarized in Table III. The phase difference χ between the Raman tensor elements a and b is about 93° and 104° for parallel and crossed polarization vectors, respectively. It was shown by Strach *et al.* that the choice of parameters a and b and the phase χ is not unique for perpendicularly polarized polarization vectors of the incoming laser and the scattered radiation.[21] Thus the ratios for crossed polarization vectors in Table III are not well defined, but they are in good agreement with the ratios estimated by the results of parallelly aligned incident and scattered polarization vectors.

Since all phonon modes of c-plane faced samples are angle independent, the relative values of the Raman tensor elements for the c-plane ZnO sample can be estimated by dividing the square root of the mean values of the fitted areas. This was only done for the A_1(LO) and E_2^{high} phonon modes for the parallel alignment of the polarization vectors because in the case of crossed polarization vectors the A_1(LO) phonon is not allowed. The result is also given in Table III. The ratios of $\lvert a/d\rvert$ for the A_1(TO) and A_1(LO) phonon modes differ by a factor of about 0.6, which is caused by their difference in bond polarity.

The relative values for the two different polarization configurations in Table III are close to each other but not within their standard errors. This might be caused by the assumption of a linear background.

V. SUMMARY

The selection rules for crystals in wurtzite structure were calculated by parameterizing the incoming and scattered polarization vectors. Angle-dependent Raman spectra for

a- and *c*-plane ZnO samples were recorded, observed modes were discussed, and the angle variations were compared with the calculated scattering intensities of allowed phonon modes, yielding the relative values of the Raman tensor elements of various ZnO phonon modes. Furthermore the assignments of Raman modes were reviewed and confirmed.

*thomas.sander@physik.uni-giessen.de

[1]T. C. Damen, S. P. S. Porto, and B. Tell, Phys. Rev. **142**, 570 (1960).
[2]C. A. Arguello, D. L. Rousseau, and S. P. S. Porto, Phys. Rev. **181**, 1351 (1969).
[3]R. H. Callender, S. S. Sussman, M. Selders, and R. K. Chang, Phys. Rev. B **7**, 3788 (1973).
[4]B. H. Bairamov, A. Heinrich, G. Irmer, V. V. Toporov, and E. Ziegler, Phys. Status Solidi B **119**, 227 (1983).
[5]L. Bergman, X.-B. Chen, J. Huso, J. L. Morrison, and H. Hoeck, J. Appl. Phys. **98**, 093507 (2005).
[6]J. F. Scott, Phys. Rev. B **2**, 1209 (1970).
[7]J. M. Calleja and M. Cardona, Phys. Rev. B **16**, 3753 (1977).
[8]D. G. Mead and G. R. Wilkinson, J. Raman Spectrosc. **6**, 123 (1977).
[9]R. Cuscó, E. Alarcón-Lladó, L. Artus, J. Ibáñez, J. Jiménez, B. Wang, and M. J. Callahan, Phys. Rev. B **75**, 165202 (2007).
[10]S. S. Mitra, O. Brafman, W. B. Daniels, and R. K. Crawford, Phys. Rev. **186**, 942 (1969).
[11]F. Decremps, J. Pellicer-Porres, A. M. Saitta, J.-C. Chervin, and A. Polian, Phys. Rev. B **65**, 092101 (2002).
[12]J. S. Reparaz, L. R. Muniz, M. R. Wagner, A. R. Goni, M. I. Alonso, A. Hoffmann, and B. K. Meyer, Appl. Phys. Lett. **96**, 231906 (2010).
[13]G. Callsen, J. S. Reparaz, M. R. Wagner, R. Kirste, C. Nenstiel, A. Hoffmann, and M. R. Phillips, Appl. Phys. Lett. **98**, 061906 (2011).
[14]J. Serrano, A. H. Romero, F. J. Manjón, R. Lauck, M. Cardona, and A. Rubio, Phys. Rev. B **69**, 094306 (2004).
[15]Y. J. Xing, Z. H. Xi, Z. Q. Xue, X. D. Zhang, J. H. Song, R. M. Wang, J. Xu, Y. Song, S. L. Zhang, and D. P. Yu, Appl. Phys. Lett. **83**, 1689 (2003).
[16]H. T. Ng, B. Chen, J. Li, J. Han, M. Meyyappan, J. Wu, S. X. Li and E. E. Haller, Appl. Phys. Lett. **82**, 2023 (2003).
[17]K. A. Alim, V. A. Fonoberov, and A. A. Balandin, Appl. Phys. Lett. **86**, 053103 (2005).
[18]K. A. Alim, V. A. Fonoberov, M. Shamsa, and A. A. Balandin, J. Appl. Phys. **97**, 124313 (2005).
[19]R. Loudon, Adv. Phys. **13**, 423 (1964).
[20]J. Serrano, F. J. Manjón, A. H. Romero, F. Widulle, R. Lauck, and M. Cardona, Phys. Rev. Lett. **90**, 055510 (2003).
[21]T. Strach, J. Brunen, B. Lederle, J. Zegenhagen, and M. Cardona, Phys. Rev. B **57**, 1292 (1998).